

This work was written as part of one of the author's official duties as an Employee of the United States Government and is therefore a work of the United States Government. In accordance with 17 U.S.C. 105, no copyright protection is available for such works under U.S. Law.

Public Domain Mark 1.0

<https://creativecommons.org/publicdomain/mark/1.0/>

Access to this work was provided by the University of Maryland, Baltimore County (UMBC) ScholarWorks@UMBC digital repository on the Maryland Shared Open Access (MD-SOAR) platform.

Please provide feedback

Please support the ScholarWorks@UMBC repository by emailing scholarworks-group@umbc.edu and telling us what having access to this work means to you and why it's important to you. Thank you.

JGR Space Physics

RESEARCH ARTICLE

10.1029/2024JA032909

Key Points:

- Plasma clouds (fragments) experience a significant slowdown when moving through magnetosheath plasmas
- Wave-particle interactions provide a strong phase mixing between plasma clouds and magnetosheath, and magnetospheric plasmas
- 3-D hybrid modeling and spacecraft observations provide the mass, momentum and energy transport from the magnetosheath to magnetosphere

Correspondence to:

A. S. Lipatov,
alipatov@umbc.edu

Citation:

Lipatov, A. S., Avanov, L. A., Giles, B. L., & Gershman, D. J. (2024). Hybrid kinetic modeling of the magnetosheath impulsive plasma cloud penetration through the magnetopause and comparison with MMS and other spacecraft observations. *Journal of Geophysical Research: Space Physics*, 129, e2024JA032909. <https://doi.org/10.1029/2024JA032909>

Received 26 MAY 2024
Accepted 9 JUL 2024

© 2024. The Author(s).

This is an open access article under the terms of the [Creative Commons Attribution-NonCommercial-NoDerivs License](#), which permits use and distribution in any medium, provided the original work is properly cited, the use is non-commercial and no modifications or adaptations are made.

Hybrid Kinetic Modeling of the Magnetosheath Impulsive Plasma Cloud Penetration Through the Magnetopause and Comparison With MMS and Other Spacecraft Observations

A. S. Lipatov^{1,2} , L. A. Avanov^{2,3} , B. L. Giles^{2,4} , and D. J. Gershman² 

¹University of Maryland Baltimore County, Baltimore, MD, USA, ²NASA Goddard Space Flight Center, Greenbelt, MD, USA, ³University of Maryland, College Park, MD, USA, ⁴Polar Winds Research, Rockville, MD, USA

Abstract This research examines the plasma processes under penetration of the plasma clouds (plasmoids) across the magnetopause which is modeled as a tangential discontinuity (TD). Cases with the parallel magnetic field in both sides out of the TD are under investigation. Plasma parameters and magnetic field were chosen from the MMS mission and other spacecraft observations. The results are important for understanding the following basic space plasma physics problems: (a) plasma cloud deformation and strong phase mixing with magnetospheric plasma; (b) the transfer of mass, momentum and energy of magnetosheath and magnetic cloud plasma into magnetospheric plasmas; (c) necessary conditions for plasma cloud penetration via the magnetopause; (d) wave generation by plasma clouds inside the magnetopause.

1. Introduction

The Chapman-Ferraro problem for the non-stationary interaction between the solar wind and magnetosphere have stood for several decades. One task to solve the problem is to study the effects of plasma cloud penetration via the magnetopause, namely, the mass, momentum, and energy transfer from the magnetosheath into the inner magnetosphere; plasma cloud deformation and destruction; phase mixing between the magnetosheath and magnetospheric plasma; excitation of electromagnetic instabilities; particle heating; and acceleration.

Magnetosheath plasma clouds have been observed by several missions: INTER-BALL-1, MAGION-4, Cluster, THEMIS, and MMS (Amata et al., 2011; Archer et al., 2012; Burch et al., 2016; Escoubet et al., 2020; Hietala et al., 2009; Hietala & Plaschke, 2013; Nemecek et al., 1998; Savin et al., 2008; Shue et al., 2009). While they found ion flux enhancements, there was little to inform about any separate enhancements in plasma density and velocity. The observations led to the conclusion that the enhancements in ion kinetic energy resulted from the interaction between the distinct IMF variations and the bow shock. Jarvinen et al. (2018) suggested another mechanism for the formation of the magnetosheath energetic protons observed. Their simulation of plasma cloud transfer to the magnetosheath from the magnetopause during a FTE associated with magnetic field reconnection demonstrated proton accelerations of 30 keV in the magnetosheath as was observed by the Cluster spacecraft.

Plasma cloud size was found to be up to $\approx 10 R_E$ across the magnetic field and larger by a factor of 3–4 along the magnetic field, while the speed exceeded the ambient plasma velocity by as much as 10%. Archer et al. (2012), using THEMIS observations, found a smaller plasma cloud size $\approx 1 R_E$ along the flow and $\approx 0.2 - 0.5 R_E$ across the flow. Plasma cloud anisotropies (parallel and perpendicular flow) estimated by Escoubet et al. (2020) from Cluster and MMS observations were: $D_{\parallel}(C1) = 1.2 R_E$; $D_{\perp}(C1) = 2.4 R_E$ and $D_{\parallel}(MMS1) = 2.6 R_E$; $D_{\perp}(MMS1) = 5.2 R_E$. Here, R_E denotes the radius of the Earth, subscripts “C1” and “MMS1” denote Cluster and MMS spacecrafts. The D_{\perp} size estimation was based on the assumption that the ratio between D_{\parallel} and D_{\perp} of ≈ 0.5 by Plaschke et al. (2016). The Cluster and MMS observations also showed that the plasma cloud speed may reach up to 380 km/s in the X-direction and a wide range of plasma cloud density, up to 43 cm^{-3} , inside the magnetosheath. Cluster and MMS also observed magnetopause motion with speeds along the normal of $\pm 140 \text{ km/s}$ and from 110 km/s to -177 km/s , respectively. The observations did not indicate pressure pulses in the solar wind were correlated with the pressure pulses downstream of the quasi-parallel bow shock. Archer et al. (2012) concluded these pressure pulses maybe produced by IMF jumps reconstructing the bow shock from quasi-perpendicular to quasi-parallel or vice versa.

Recently, several plasma clouds were discovered inside the magnetosheath on 07/03/2016 from 00:00:20 to 01:00:00 UT. The Fast Plasma Investigation (FPI) (Pollock et al., 2016) and MMS flux-gate magnetometers

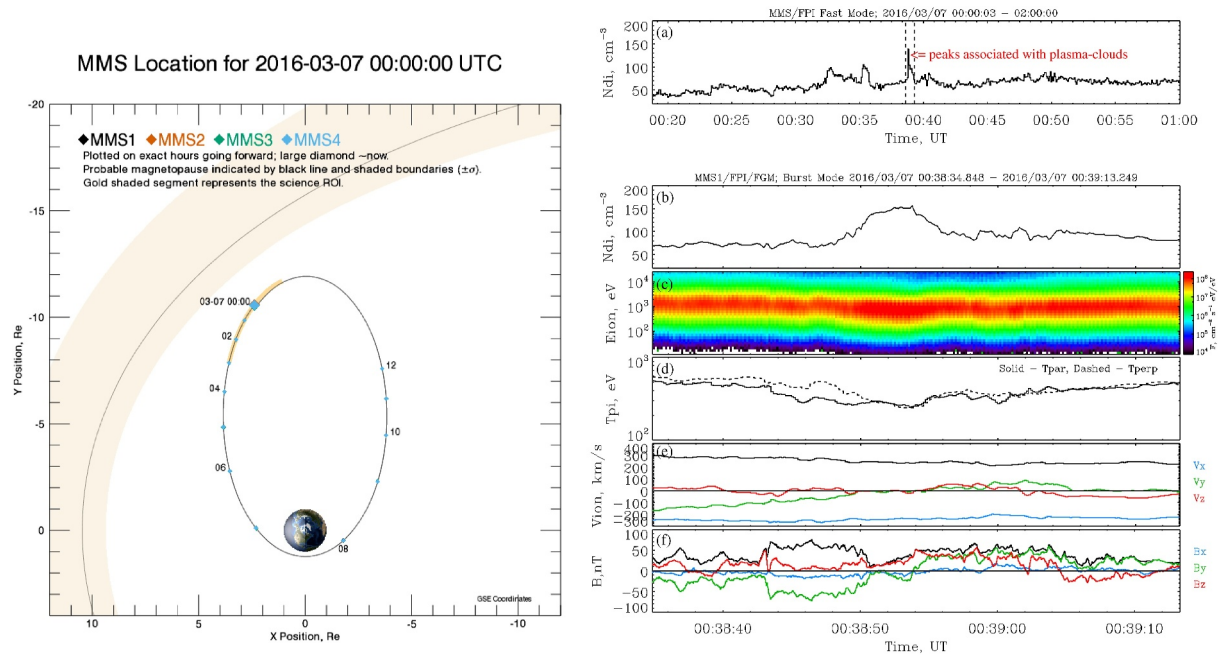


Figure 1. Left—MMS spacecraft orbit. Right—MMS Fast Mode observation: Ion density profile (a); MMS Burst Mode observation: Ion density profile (b), Ion energy flux profile (c), Ion parallel and perpendicular temperature profiles (d), Ion velocity profiles (e), and Magnetic field profiles (f).

(Russell et al., 2016) showed that the density peaks in the range from $\approx 100 \text{ cm}^{-3}$ to $\approx 160 \text{ cm}^{-3}$ (Figure 1a). Burst mode data for the time interval from 07/03/2016 00:38:36 to 07/03/2016 00:39:14 revealed important features in the plasma and magnetic field distribution inside the plasma cloud and nearby magnetosheath plasma that had not been available in previous studies. Figure 1b shows peak density variations from 70 cm^{-3} – 160 cm^{-3} . Figure 1c presents the ion energy flux showing a slightly lower energy of the cloud ions (from $3 \times 10^2 \text{ eV}$ to $\approx 2 \times 10^3 \text{ eV}$) in comparison with ion energies in the magnetosheath. The ion temperature profile is shown in Figure 1d, note the lower ion temperatures inside the plasma cloud as compared to the magnetosheath. The value of the $T_{i,\perp}$ is close to the $T_{i,\parallel}$ except in regions outside the cloud where there is strong electromagnetic wave generations.

The components of cloud speed are $V_x \approx -240 \text{ km/s}$, $V_y \approx 0 \text{ km/s}$ and $V_z \approx 0 \text{ km/s}$. Upstream of the cloud, the V_y component of the magnetosheath plasma speed reaches values from 0 km/s to $\approx -160 \text{ km/s}$, Figure 1e, along with the excitation of transverse waves, Figure 1f. Plasma cloud sizes are: $D_x \approx 2,400 \text{ km}$ in the X-direction, $D_y \approx 1,000 \text{ km}$ in the Y-direction and $D_z \approx 200 \text{ km}$ in the Z-direction.

Early studies of solar wind plasma penetration of the magnetopause focused on theoretical issues (Cowley, 1986; Heikkila, 1982; Lemaire, 1977, 1985; Lemaire & Roth, 1978; Lundin & Dubinin, 1984; Lyatsky et al., 2016; Owen & Cowley, 1991; Schindler, 1979). explored the global interaction (Dai & Woodward, 1994, 1995; Ma et al., 1991; Suzuki et al., 1998) although those models were not able to include wave-particle interactions, which are critical for phase mixing by producing the mass, momentum, and energy transfer from the magnetosheath/plasma cloud into the magnetospheric plasma.

2-D Hall-MHD simulations by Huba (1996) demonstrated the complicated structure of the combined magnetosheath-cloud plasma–magnetospheric plasma interface when plasmoids penetrate via a tangential discontinuity (TD). The evolution of the combined structure remained symmetric across the propagation direction. The Hall-MHD case with an asymmetric antiparallel magnetic field showed the evolution was much like the ideal MHD case. The Hall-MHD case with parallel magnetic fields produced a plasma configuration quite different from the ideal MHD case.

2.5-D hybrid simulation by Savoini et al. (1994) produced results close to the Hall-MHD modeling by Huba (1996). They demonstrated the importance of the ion particle dynamics inside small-scale perturbations with length scales of the ion inertial length or the ion gyroradius. Lipatov et al. (1994) and Lipatov (1996, 2002) performed 2.5-D hybrid kinetic simulations of supersonic plasma cloud penetration through a TD. They observed

the generation of strong whistler/Alfvén waves propagating along the magnetic field in the vicinity of the TD. The generation of these waves was not observed in Savoini et al. (1994) or Huba (1996) possibly due to limitations on the size of the simulation box along the surface of the TD.

Omidi et al. (2016) performed a global 2.5-D hybrid simulation of the impact of hot flow anomalies and magnetosheath cavities on magnetopause position. The simulated pressure variations in the magnetosheath result in the magnetopause motion in Sun-Earth direction. A global 2.5-D hybrid-Vlasov (Vlasiator) statistical simulation of the jet cluster by Palmroth et al. (2021) compared MMS observations with magnetosheath jets and plasmoid cluster evolution with time. They found a sharp jump in the parameters of the jets at the bow shock, which decreases toward the magnetopause. They also found that magnetosheath jet configurations are depended on the solar wind Alfvén Mach number.

3-D electro-static modeling of plasma cloud penetration through the magnetopause was performed by Gunell et al. (2008, 2009). They found interesting results for plasma cloud deformation and wave excitation although for short time (lower-hybrid frequency range) and spatial scales of 10–100 km. They concluded that for cases with southward IMF and large plasma cloud the full 3-D electromagnetic code must be used for simulation. Voitu and Echim (2016) presented a 3-D electromagnetic PIC simulation of the an isolated plasmoid through a TD. Their results about plasmoid deformation were not able to account for effects of the background plasma inside the transition from the magnetosheath to magnetosphere.

Because the ion gyroradius is comparable with the thickness of plasma structures and the size of interpenetration features of the different species of plasma, hybrid modeling can be expected to significantly extend these prior the above problems results. Building on these 2.5-D and 3-D hybrid, and 3-D electrostatic, and electromagnetic simulations, this study applies a 3-D hybrid kinetic simulation to study plasma cloud transfer across the magnetopause, for various configurations of the magnetosheath and magnetopause, and for the full range of parameters that have been observed in the plasma clouds.

In this publication the initial configuration of the magnetopause will be modeled as a tangential discontinuity (TD) with zero bulk velocity of the plasma in the magnetosheath and magnetosphere. This includes examinations of the transfer of mass, and momentum and energy from the magnetosheath into the magnetosphere, including strong phase mixing with magnetospheric plasma, and the necessary condition for cloud transfer across the magnetopause. A more complicated model that includes non-zero initial bulk velocity of the magnetosheath plasma and magnetic field reconnection is under development for a future publication.

The paper has the following sections: “Introduction,” “Computational model description” where the hybrid model and equations are described in detail, “Results” where the main simulation results provided and the analysis of the wave-particle interactions and comparisons with spacecraft observations are discussed, and “Conclusions.”

2. Computational Model Description

2.1. Hybrid Kinetic Model and Formulation of the Problem

The study of plasma cloud penetration through the magnetopause, which is assumed to be a tangential discontinuity (TD), is performed with use of a hybrid quasi-neutral model. The model employs the kinetic (particle) approach for ion dynamics, whereas the fluid approach is used for the electron dynamics.

The scheme of the computational model which describes the initial configuration of the magnetosheath, plasma cloud and magnetosphere is presented in Figure 2. In the modeling the X axis is directed along the initial speed of the plasma cloud inward to the magnetopause. The Y and Z axes are perpendicular to the X axis so that they complete the right-handed coordinate system. The initial location of the cloud center is the following: $x = 0$ L, $y = 0$ L and $z = 0$ L.

The ion distribution function $f_s(t, \mathbf{x}, \mathbf{v})$ is described by the Vlasov equation as documented in Lipatov and Sibeck (2020) and Lipatov et al. (2005, 2006):

$$\frac{\partial}{\partial t} f_s + \mathbf{v} \frac{\partial}{\partial \mathbf{x}} f_s + \frac{\mathbf{F}}{M_s} \frac{\partial}{\partial \mathbf{v}} f_s = 0, \quad (1)$$

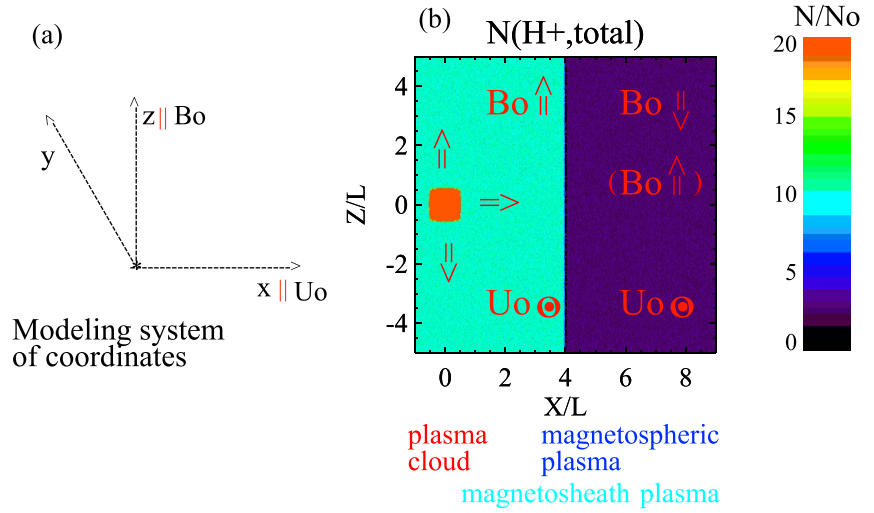


Figure 2. Set up the plasma cloud and ambient magnetosheath and magnetospheric plasma configuration for our modeling. Initial location of the plasma cloud at $X/L = 0$.

where \mathbf{F} denotes the electric and magnetic forces acting on the ions and index s denotes the ion species. Note that the terms for ion collisions, the ion production by ionization and charge exchange, and the ion loss due to charge exchange are dropped from above equation. In our simulation we use the standard PIC method for ion dynamics instead of the Vlasov equation.

The ion particle motion equations are the following:

$$\frac{d\mathbf{r}_{s,l}}{dt} = \mathbf{v}_{s,l}; \quad \frac{d\mathbf{v}_{s,l}}{dt} = \frac{e}{M_s} \left(\mathbf{E} + \frac{\mathbf{v}_{s,l} \times \mathbf{B}}{c} \right). \quad (2)$$

We assumed here that the ion charge state is $Z_s = 1$ and ion masses are $M_1 = M_{H^+}$ for the magnetospheric plasma, $M_2 = M_{H^+}$ for magnetosheath plasma, and $M_3 = M_{H^+}$ for the plasma cloud. l denotes the ion particle index.

Ampère's law in the nonradiative limit and Faraday's law has the following forms:

$$\frac{4\pi}{c} \mathbf{J} = \nabla \times \mathbf{B}; \quad (3)$$

$$\frac{1}{c} \frac{\partial \mathbf{B}}{\partial t} + \nabla \times \mathbf{E} = 0. \quad (4)$$

The total current is given by

$$\mathbf{J} = \mathbf{J}_e + \mathbf{J}_i; \quad \mathbf{J}_i = \sum_{s=1}^3 en_s \mathbf{U}_s = en_i \mathbf{U}_i, \quad (5)$$

where \mathbf{U}_s is the bulk velocity of ions of the species s .

We also assume plasma quasi-neutrality

$$n_e = \sum_{s=1}^3 n_s. \quad (6)$$

The electric field was calculated from the standard generalized Ohm's law (see e.g., Braginskii, 1965):

$$\mathbf{E} = \frac{1}{en_e c} (\mathbf{J}_e \times \mathbf{B}) - \frac{1}{en_e} \nabla p_e, \quad (7)$$

where $p_e = nm_e \langle v_e'^2 \rangle / 3 = n_e k_B T_e$, and v_e' are the scalar electron pressure and the thermal velocity of electrons, and the electron current is estimated from Equation 5.

Because we assume the electron heating due to collisions with ions is very small, the electron fluid is considered adiabatic. For simplicity then, we assume the total electron pressure may be represented as a sum of the partial pressures of all electron populations:

$$p_e \propto \frac{(\beta_{e,M-SPH} n_{i,M-SPH}^{5/3} + \beta_{e,M-SH} n_{i,M-SH}^{5/3} + \beta_{e,P-C} n_{i,P-C}^{5/3})}{\beta_{e,M-SPH}}, \quad (8)$$

where $\beta_{e,M-SPH}$, $\beta_{e,M-SH}$, and $\beta_{e,P-C}$ denote electron magnetospheric, magnetosheath and plasma cloud betas. We also assume that $n_{e,M-SPH} = n_{i,M-SPH}$, $n_{e,M-SH} = n_{i,M-SH}$, and $n_{e,P-C} = n_{i,P-C}$.

This model describes the wave-particle interactions on the ion scale ($\rho_{ci} = U_0/\Omega_i$ and $\omega \leq \Omega_i$). Here, U_0 , Ω_i and ρ_{ci} are the characteristic velocity used for normalization of the background plasma, the ion frequency and gyroradius.

Spacecraft observations in Figures 1a–1f are used as initial parameters for the modeling (00:20–01:20 UT). The peaks which correspond to the plasma clouds are marked in Figure 1c.

The following parameters were chosen for the magnetosheath plasma and magnetic field: density $N_{i,m-sh} = 10$ – 60 cm^{-3} ; thermal ion and electron velocities $V_{th,i} = 60$ – 100 km/s ; $V_{th,e} = 1,000 \text{ km/s}$; Alfvénic velocity $V_A \approx (80$ – $200) \text{ km/s}$; and the incoming magnetic field $B = (0; 0; 30) \text{ nT}$.

The thermal ion and electron velocities in the magnetosphere are 100 km/s and $2,200 \text{ km/s}$, respectively. The value of the plasma density is 2.4 cm^{-3} . The initial value of the magnetospheric magnetic field assumed to be $B \approx 60 \text{ nT}$. The value of plasma betas and the Alfvén speed in the magnetosphere are $\beta_i = 0.0125$, $\beta_e = 0.0024$, and $V_A = 780 \text{ km/s}$.

2.2. Initial and Boundary Conditions

The following initial conditions are chosen: a homogeneous ambient magnetosheath and magnetospheric plasma flow with initial bulk velocity $\mathbf{U}_0 = 0$; magnetic and electric fields with values $\mathbf{B} = \mathbf{B}_0$ and $\mathbf{E} = -\mathbf{U}_0 \times \mathbf{B}_0/c$. The magnetosheath and magnetospheric ion velocity distribution functions (VDFs) are approximated with Maxwellian distributions. The initial profile of the magnetopause (TD) was chosen as a transition between the magnetosheath and magnetosphere with a width $\Delta_{TD} \approx 2 \times \Delta x$, where Δx denotes the size of the spatial grid in the X direction. Initially, the value of the total (plasma and magnetic field) pressure in the magnetosheath plasma is equal to one in the magnetospheric plasma. At the first stage of the modeling the TD evolves in time self-consistently so that the TD thickness becomes $\approx 200 \text{ km}$ far from the plasma cloud location.

In our modeling we superimposed cloud ions on the magnetosheath plasma. Initially the cloud ions have no radial speed and the cloud expansion is driven by a strong gradient in the center of cloud. Cloud expansion and motion produce a depletion in the ambient background density and the cloud-ambient background plasma system forms a self-consistent interface very quickly. The initial values of the cloud speed are speed $U = (-350[700], 0, 0) \text{ km/s}$; the thermal ion and electron velocities $V_{th,i} = 1$ – 50 km/s and $V_{th,e} = 2,400 \text{ km/s}$. We investigated various initial distributions of the cloud density and the initial location inside the magnetosheath. The cases exhibiting the best agreement with the observations are presented here.

A Gaussian distribution with standard deviation $\sigma = 0.44 L = 200$ – 400 km was used for approximation of the initial profile of the cloud density. The peak of the distribution is chosen as $N_{\max} \approx 60$ – 110 cm^{-3} .

A variable mass of macro-particles acts to reduce “shot” noise in the cloud density and velocity profiles (Lipatov, 2012). The data from MMS3 are used for the modeling. Due to the small spacecraft separation ($< 15 \text{ km}$) the data from the other MMS spacecraft are approximately the same on the spatial scale of the processes studied here.

Table 1
Modeling Parameters

Case, L(km)	$U_{0,cloud}$ (km/s)	R_{ci} (km)	$V_{th,i,m-sh}/W_0$	N_{cloud} (cm ⁻³)	$\frac{N_{cloud}}{N_{m-sh}}$
Run	N_{m-sh} (cm ⁻³)	$\Delta_{cloud-mp}$ (km)	$V_{th,i,cloud}/W_0$	B_{m-sh} (nT)	Effectivity
1, $L = 200$	700	230	0.6	≈ 110	1.8
ghkhha	60	1,000	0.1	30	$\approx 100\%$
2, $L = 400$	700	230	1.47	≈ 110	11
ghcc	10	2,000	0.1	30	$\approx 100\%$
3, $L = 200$	300	100	0.6	≈ 110	1.8
ghkhbb	60	600	0.1	30	$\approx 50\%$
4, $L = 400$	350	116	1.47	≈ 110	11
ghjcc	10	2,000	0.1	10	$\approx 100\%$
5, $L = 200$	300	100	0.6	≈ 110	1.8
ghkhh	60	1,000	0.1	30	$\approx 10\%$
6, $L = 400$	300	100	0.6	≈ 60	1
ghkk	60	600	0.1	30	$\approx 0\%$

Note. Effectivity of mass, momentum and energy transfer through TD.

Our computational model includes the super/trans/sub-Alfvénic(sonic) regime in the transition from the magnetosheath to the magnetosphere so that, in principle, we have to use an infinite size of the computational domain in the trans/sub-Alfvén(sonic) regions to avoid a reflection of the wave and plasma flux at the flank and downstream boundaries. The unperturbed ion VDF's flux are injected into the computational domain at the flank and rear (right) boundaries (Figure 2).

Since we used the shifted grid point for the magnetic and electric field computation (see, e.g. Lipatov, 2002) the values of the electric field outside the left, flank, and back boundaries (Figure 2) were equal to the undisturbed external plasma parameters. There are no specific boundary conditions at the interface between the plasma cloud, magnetosheath and magnetosphere because our model describe the interpenetration flows for those ion species. The magnetic field perturbations are allowed to propagate across the back boundary by the use of the “Sommerfeld” radiation condition (Schot, 1992).

The following dimensions of the computational domain are used in the modeling: ($DX = 30 L$, $DY = 30 L$, $DZ = 30 L$). Here, $L = 200$ – 400 km denotes the effective length. The grid points of $301 \times 301 \times 301$ and $301 \times 201 \times 201$ cover the computational domain. The cloud, magnetosheath and magnetospheric ion VDFs are calculated with the particle-in-cell algorithm. This approach provides a good numerical resolution with ≈ 50 and ≈ 80 – 200 macro-particle per cell for the cloud and magnetosheath, and magnetospheric ions. The following time steps.

$\Delta t_p \leq \min(\Delta x, \Delta y, \Delta z)/(16v_{max})$ and $\Delta t_{EB} = \Delta t_p/16$ are used for particle and electromagnetic field calculation, where $\Delta x, \Delta y, \Delta z$ are the cell sizes. Small time steps provide better algorithm convergence in modeling a plasma system with low density.

Macro-particle pushing were produced with a leap-frog trapezoid scheme whereas electromagnetic equation computation was produced with an implicit scheme (Lipatov, 2002). This algorithm has demonstrated effective performance in the modeling of the plasma environment near weak comets and planetary moons, and transmitted shock and plasma clouds inside the magnetosphere (Lipatov et al., 2022 and references therein).

3. Results

The structure of the plasma cloud and the response of the ambient plasma under penetration through the TD are key factors for understanding the wave-particle interactions which result in phase mixing, particle heating and acceleration, and low-frequency wave excitation. Here we discuss the results of the modeling and the comparisons with MMS observations in detail. In Table 1 we summarize the parameters of the models that were investigated.

In Table 1, $U_{0,cloud}$ (km/s) is the initial speed of the cloud; N_{m-sh} (cm^{-3}) is the plasma density in the magnetosheath; R_{ci} (km) is the ion gyroradius; Δ_{c-mp} (km) is the initial distance between the cloud and magnetopause; $V_{th,i,m-sh}/W_0$ and $V_{th,i,cloud}/W_0$ are the thermal velocity of the ions inside the magnetosheath and the clouds; $W_0 = 100$ km/s is the characteristic velocity; L is the characteristic length, N_{cloud} (cm^{-3}) and B_{m-sh} (nT) are initial values of the cloud density and magnetic field in the magnetosheath. Note that the initial value of the magnetosheath ion thermal velocity $V_{th,i,m-sh}$ is different from the one in the preliminary modeling (Lipatov et al., 2024).

3.1. High-Speed Plasma Cloud Penetration Through TD

The physics of the high speed plasma cloud penetration through the tangential discontinuity strongly depends on the value of the magnetosheath density because the plasma cloud slows while moving inside the magnetosheath. Plasma cloud slowdown within an ambient dense plasma was observed in the hybrid modeling by Bashurin et al. (1983) and Berezin et al. (1992). In our modeling we separately consider the case with a high and low density magnetosheath.

3.1.1. High-Density Magnetosheath

In this case (Case 1, Table 1) we use the following parameters for the modeling: characteristic spatial length $L = 200$ km and cloud speed $U_x = 700$ km/s. The initial plasma density and ion thermal velocity are: (a) Plasma cloud— $N_{i,cloud} \approx 110 \text{ cm}^{-3}$ and $V_{th,i} \approx 10$ km/s; (b) Magnetosheath— $N_{i,cloud} \approx 60 \text{ cm}^{-3}$ and $V_{th,i} \approx 60$ km/s; (c) Magnetosphere— $N_{i,cloud} \approx 2.4 \text{ cm}^{-3}$ and $V_{th,i} \approx 100$ km/s. The plasma cloud is expected to experience a slowdown due to an interaction with magnetosheath plasma. The slowdown is one of the key factors that controls the speed of the plasma clouds upstream the TD. In the case of higher initial speeds of the plasma cloud (700 km/s) and a high density magnetosheath the modeling does not show as strong of a plasma cloud slowdown. The speed of the lead edge of the plasma cloud moves with speed of 670 km/s upstream near the TD.

Figure 3 shows 2-D cuts of the ion density for the plasma cloud, magnetosphere and magnetosheath. The plasma cloud produced a complex three-dimensional configuration when it penetrates from the magnetosheath into the magnetosphere plasma. The plasma cloud configuration is asymmetrical in the X - Y plane due to the finite ion gyroradius while it is symmetrical in the X - Z plane. The plasma cloud configuration has an expanding “mushroom-like” dense structure with a thin wake, which is extended between the head and its initial location. The size of the mushroom-like head is about $\approx 10 L = 2,000$ km in Y direction and $\approx 7 L = 1,400$ km in Z direction. Note here that a formation of the mushroom-like head was also observed in the modeling of the interaction between a drainage plume and transmitted impulses (Lipatov & Sibeck, 2020).

A portion of the magnetosheath ions which are picked up by the plasma cloud also penetrates into the magnetosphere. Penetrated magnetosheath plasma forms an irregular wide jet. Note that this 3-D modeling does not show a strong depletion in the magnetosheath plasma density due to plasma cloud motion in contrast to that observed in the 2.5-D hybrid (Savoini et al., 1994) and 2-D Hall MHD modeling (Huba, 1996). The plasma cloud creates a cavity inside the magnetosphere. The expanding plasma cloud produces a compression of magnetospheric plasma at the boundary of the cavity. At the TD one can see the motion of the portion of magnetospheric plasma in the opposite direction while the magnetosheath plasma profile has a depletion at $X < 5 L = 1,000$ km in the X - Y plane. The modeling also demonstrates deformation of the TD in the X direction which is the opposite of the shape of the TD deformation in the X - Y plane.

Figures 4a and 4b show 2-D cuts of the B_z magnetic field components in the X - Y and X - Z planes. One can see the plasma compression inside the magnetosheath and in the region where the plasma cloud penetrates inside the magnetosphere. Figure 4c shows the distribution of the total kinetic energies for the plasma cloud (solid line), magnetospheric plasma (dotted line) and magnetosheath plasma (dashed line) along the X -axis. The energies were normalized by the maximum of the kinetic energy for each species. The modeling shows that the main portion of the total kinetic energy of the plasma cloud is located inside of the mushroom-like structure. The total kinetic energy in the magnetospheric plasma grows after heating due to the interaction with the plasma cloud. The magnetosheath plasma also gains kinetic energy when it is picked up by the plasma cloud.

Figures 5–7 show the anisotropic velocity distribution functions (VDFs) for the plasma cloud ions, magnetospheric ions and magnetosheath ions in the U - V , U - W and V - W planes for the spatial sections F1, F3, F6, F12 and

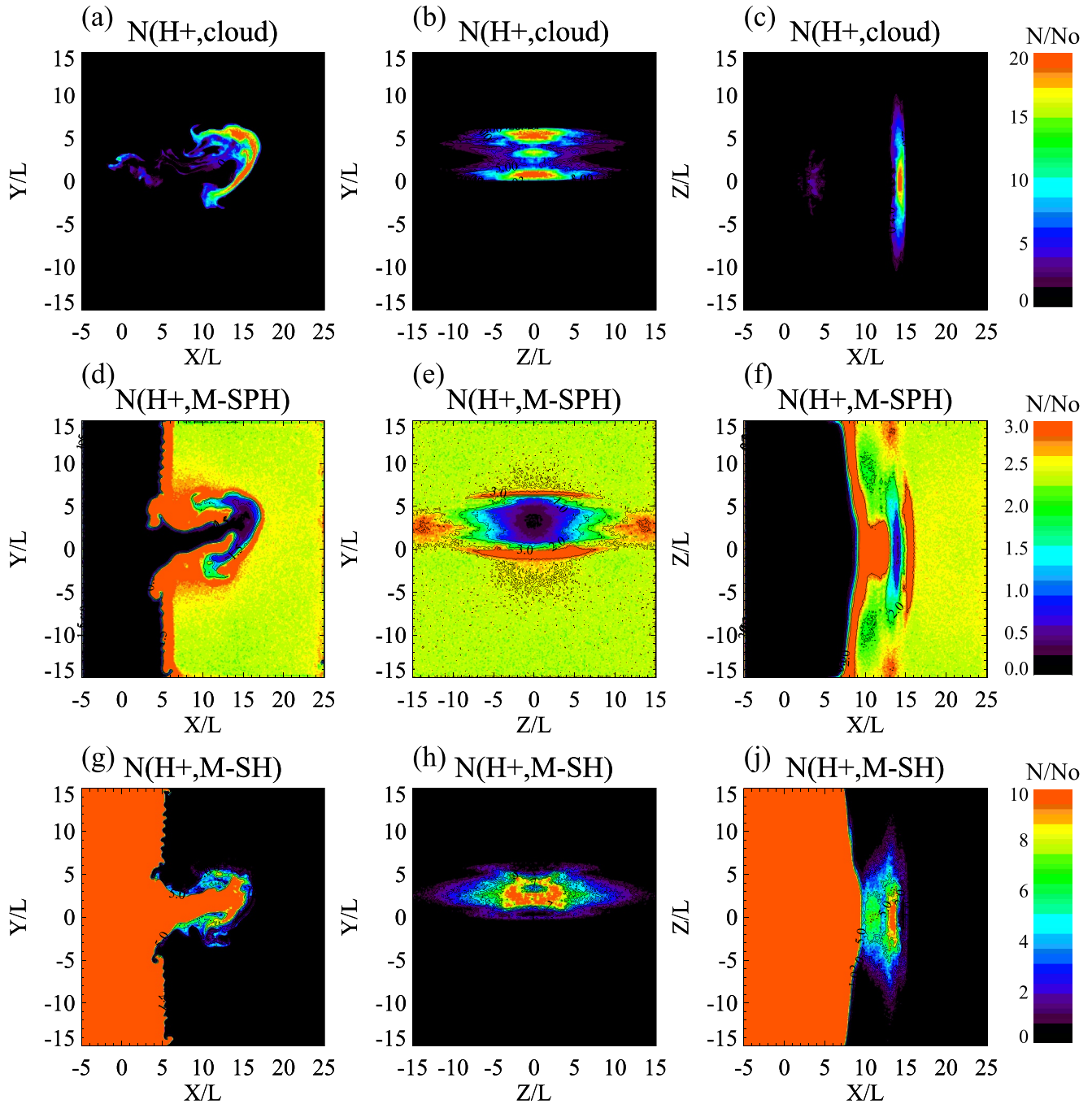


Figure 3. Dense magnetosheath and fast initial P-C speed (Case 1, Run 112ghkhha). Top: Cloud density; Middle: Magnetospheric density; Bottom: Magnetosheath density. $L = 200$ km; Cloud speed $U_x = 700$ km/s; Initial plasma density and ion thermal velocity: (a) Plasma cloud: $N_{i,\text{cloud}} \approx 110 \text{ cm}^{-3}$; $V_{th,i} \approx 10$ km/s; (b) Magnetosheath: $N_{i,m-sh} \approx 60 \text{ cm}^{-3}$; $V_{th,i} \approx 60$ km/s; (c) Magnetosphere: $N_{i,m-sph} \approx 2.4 \text{ cm}^{-3}$; $V_{th,i} \approx 100$ km/s. The middle column is located at $X \approx 15$ L and $t \approx 18$ s.

F14, Figure 5d. These VDFs were calculated with ion positions over the cube in the spatial coordinates with sizes: $\delta X = 5$ L, $\delta Y = 5$ L and $\delta Z = 0.35$ L.

The VDFs of the plasma cloud ions represent a strong core and a wide halo across the magnetic field. The ion VDFs have 2 parts in the core region for sections from F1 to F6. There are also ring-like structures in the ion VDFs in the sections from F3 to F14 in Figure 5a. Formation of the halo in the ion VDFs is a result of the interaction between the plasma cloud and the ambient background (magnetosheath and magnetospheric) plasma. The maximum value of the ion velocity in the halo is about ≈ 500 km/s and ≈ 800 km/s in the ring-like structures. The

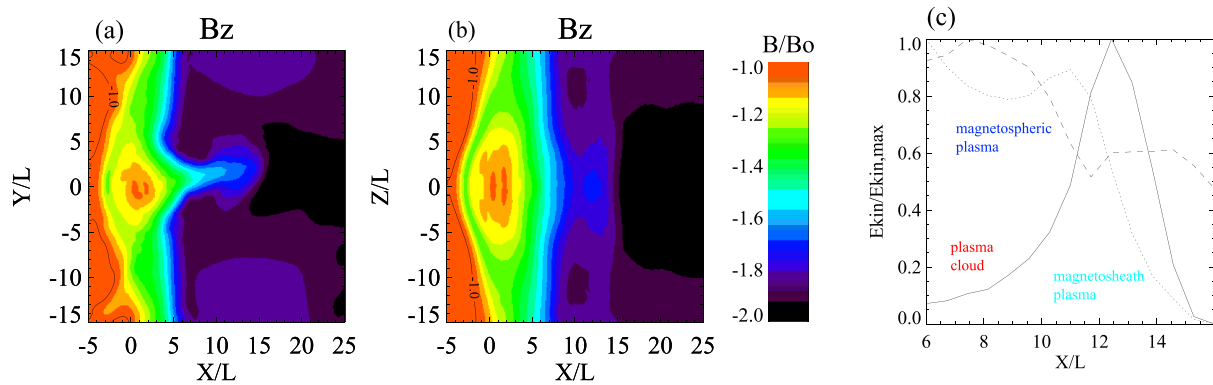


Figure 4. Left: 2-D cuts of the magnetic field component B_z for the same parameters as in Figure 3. Right: Normalized kinetic energy distribution for plasma cloud, magnetospheric and magnetosheath ions.

ion VDFs of the plasma cloud show a strong expansion of the core along the magnetic field in Figure 5b. The maximum value of the ion velocity along the magnetic field is about ≈ 250 km/s. The cloud ion VDFs demonstrated both a formation of the halo and ion expansion along the magnetic field, Figure 5c.

The VDFs of the magnetospheric ions also demonstrate a strong core and a wide halo across the magnetic field, Figure 6a. The cores of the ion VDF are quasi-symmetrical in opposite to the core of the VDF for the plasma cloud ions.

The formation of the halo in the ion VDF is a result of the interaction with the plasma cloud during penetration into the ambient background magnetospheric plasma. The maximum value of the ion velocity in the halo is about ≈ 500 – 800 km/s. Additional heating of the magnetospheric ions across the magnetic field are associated with a compression of the magnetospheric plasma in sections from F1 to F6 (see also Figure 6d). The VDFs of the magnetospheric ions also show a strong expansion of the core along magnetic field, Figure 6b. The maximum value of the ion velocity along the magnetic field is about ≈ 350 km/s. The ion VDFs demonstrate both a formation of the halo and ion expansion along the magnetic field, Figure 6c.

The VDFs of the magnetosheath ions present a strong quasi-asymmetrical core and a wide halo across the magnetic field, Figures 7a, 7b and 7c. A formation of the halo in the ion VDF is a result of the interaction with the plasma cloud during penetration into the ambient background magnetospheric plasma. The maximum value of the ion velocity in the halo across the magnetic field is about ≈ 300 – 700 km/s in the sections from F1 to F6, Figure 7a. The cooling of the magnetosheath ions across the magnetic field in sections from F1 to F6 (Figure 7d) is due to expansion inside the lower density in the magnetosphere. The VDFs of the magnetosheath ions also show a strong expansion of the core along magnetic field, Figure 7b. The ion VDFs demonstrate both a formation of the anisotropic halo and ion expansion along the magnetic field, Figure 7c. The maximum value of the ion velocity along the magnetic field is about ≈ 300 km/s.

3.1.2. Low-Density Magnetosheath

In this case (Case 2, Table 1) we use the following parameters for the modeling: characteristic spatial length $L = 200$ km and cloud speed $U_x = 700$ km/s. The initial plasma density and ion thermal velocity are the following: (a) Plasma cloud— $N_{i,cloud} \approx 110 \text{ cm}^{-3}$ and $V_{th,i} \approx 10$ km/s; (b) Magnetosheath— $N_{i,cloud} \approx 10 \text{ cm}^{-3}$ and $V_{th,i} \approx 100$ km/s; (c) Magnetosphere— $N_{i,cloud} \approx 2.4 \text{ cm}^{-3}$ and $V_{th,i} \approx 100$ km/s. The low-density magnetosheath results in a weak slowdown of the plasma cloud motion and hence a higher value of the plasma cloud speed just before the penetration across the TD. It also results in deeper plasma cloud deeper penetration through the magnetospheric plasma.

Figure 8 shows 2-D cuts of the density profiles for the cloud, magnetosphere and magnetosheath plasma. The plasma cloud configuration has a slightly oblique orientation to the X direction. The modeling does not demonstrate strong penetration of the magnetosheath plasma into the magnetosphere. In this case, the TD (magnetopause) moves in the opposite direction ($-X$ direction) due to the plasma cloud penetration into magnetopause. The TD has a strong perturbation along with Z direction.

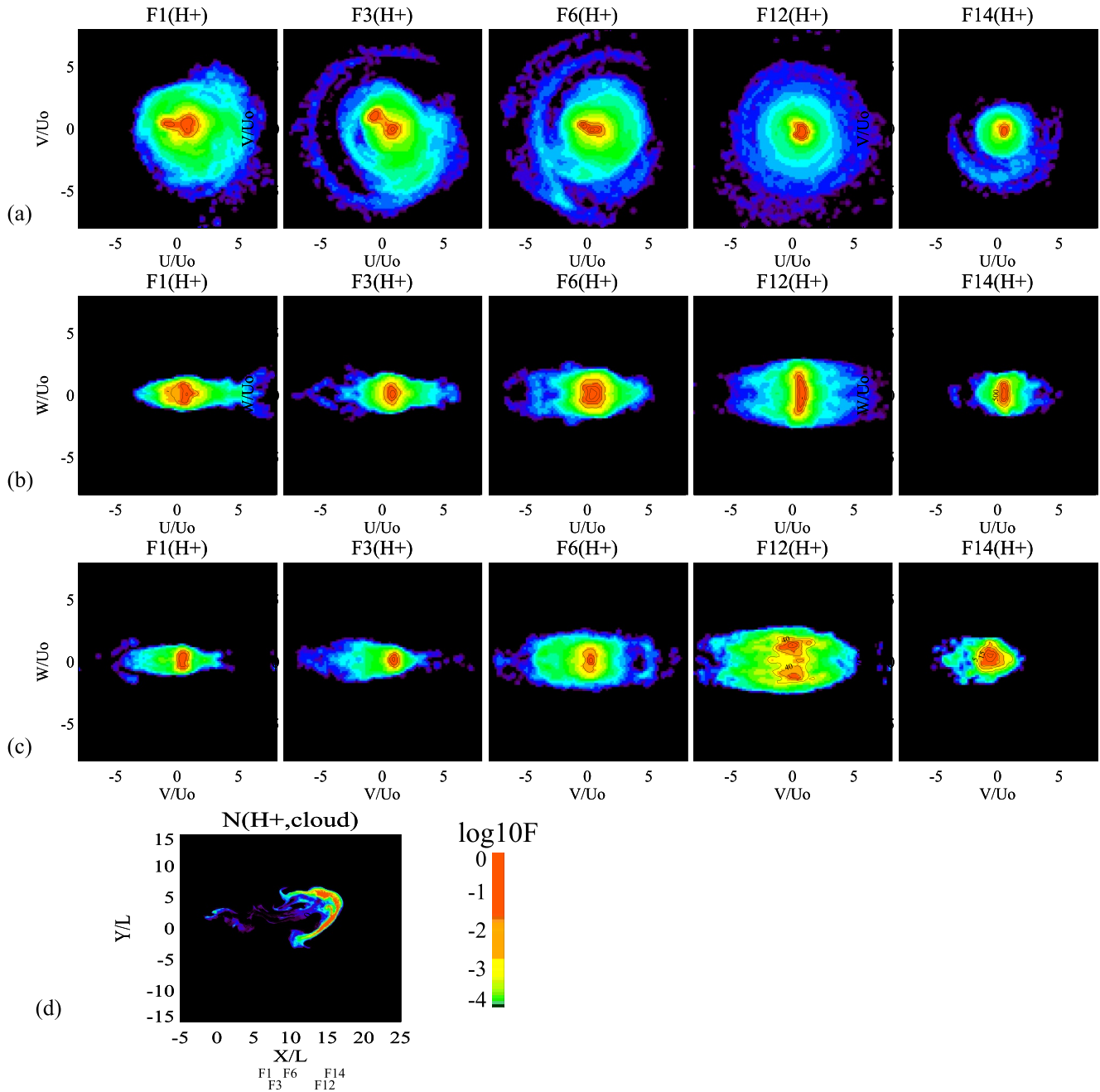


Figure 5. The plasma cloud ion (H^+) VDFs (panels (a–c)) along X axis for the same parameters as in Figure 3. Locations are shown in the cloud ion density profiles (d). $U_0 = 100$ km/s.

3.2. Moderate Speed Plasma Cloud Penetration Through TD

Next we consider plasma cloud penetration through a TD with a moderate initial speed. Remember that the initial speed of the plasma cloud is the one of the critical parameters which determines the penetration across the TD.

3.2.1. High-Density Magnetosheath but Short Initial Distance to Magnetopause

In this case (Case 3, Table 1) we use the following parameters for the modeling: characteristic spatial length $L = 200$ km and cloud speed $U_x = 700$ km/s. The initial plasma density and ion thermal velocity are: (a) Plasma cloud— $N_{i, \text{cloud}} \approx 110 \text{ cm}^{-3}$ and $V_{th,i} \approx 10$ km/s; (b) Magnetosheath— $N_{i, m-sh} \approx 60 \text{ cm}^{-3}$ and $V_{th,i} \approx 60$ km/s; (c)

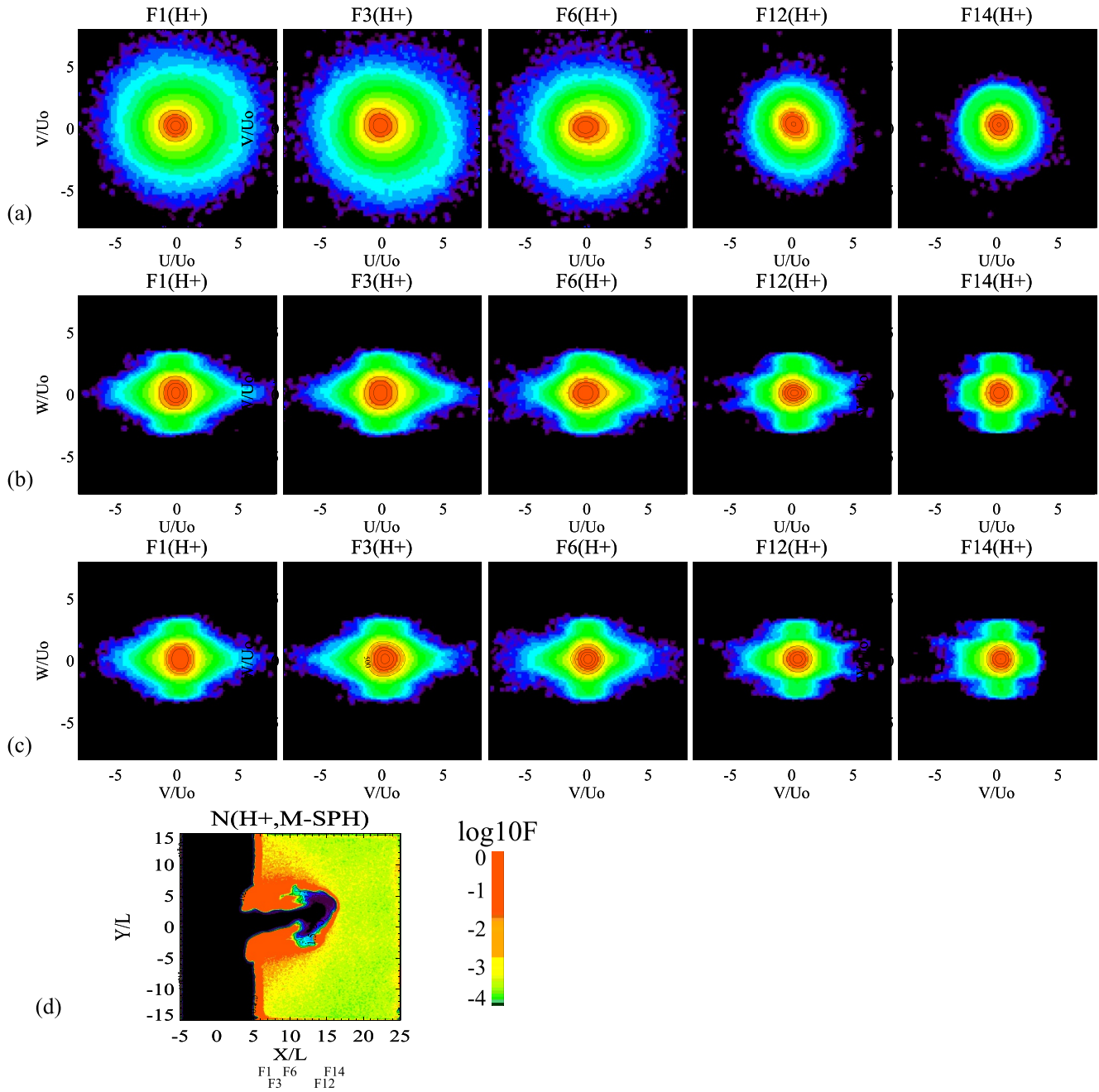


Figure 6. The magnetospheric ion (H^+) VDFs (panels (a–c)) along X axis for the same parameters as in Figure 3. Locations are shown in the magnetospheric ion density profiles (d). $U_0 = 100$ km/s.

Magnetosphere— $N_{i,m-sph} \approx 2.4 \text{ cm}^{-3}$ and $V_{th,i} \approx 100$ km/s. In this case, the initial distance between the cloud and TD was decreased by factor of 2 to reduce the cloud slowdown in the magnetosheath. Figure 9 provides the 2-D cuts of the cloud, magnetospheric and magnetosheath plasma densities for this case. The cloud penetration is not as strong as for cases with high initial cloud speed because of the strong cloud slowdown inside the magnetosheath. The average TD position does not change significantly although but it is strongly deformed in the Z direction. The thickness of the TD is increased in the X — Z plane and there is a strong pick-up of magnetosheath ions in the magnetosphere.

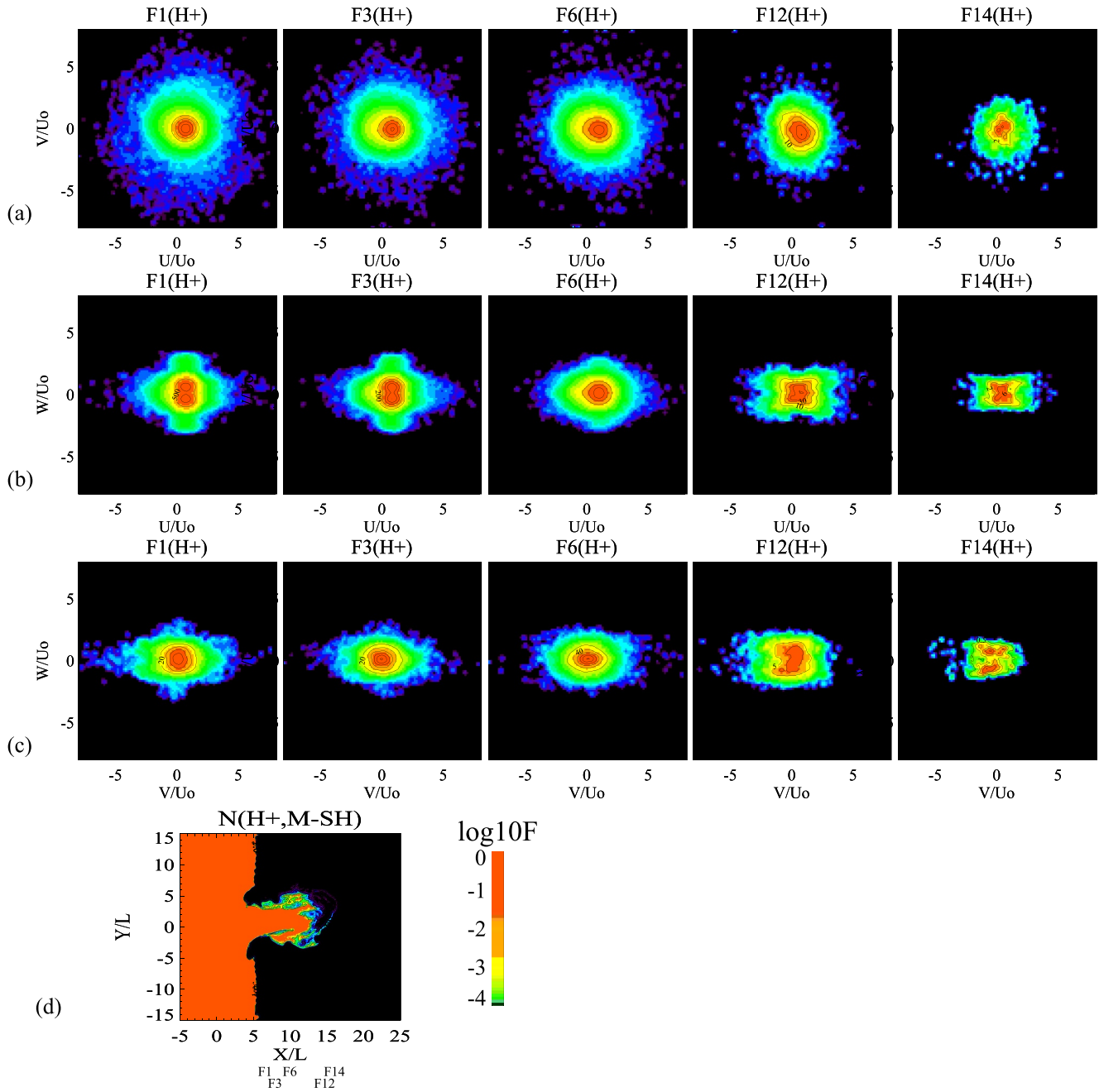


Figure 7. The magnetosheath ion (H^+) VDFs (panels (a–c)) along X axis for the same parameters as in Figure 3. Locations are shown in the magnetosheath ion density profiles (d). $U_0 = 100$ km/s.

3.2.2. Low-Density Magnetosheath

Next is the case with a low-density magnetosheath and a moderate initial speed of the plasma cloud. In this case (Case 4, Table 1) we use the following parameters for the modeling: characteristic spatial length $L = 400$ km and cloud speed $U_X = 350$ km/s. The initial plasma density and ion thermal velocity are: (a) Plasma cloud— $N_{i,cloud} \approx 110 \text{ cm}^{-3}$ and $V_{th,i} \approx 20$ km/s; (b) Magnetosheath— $N_{i,m-sh} \approx 10 \text{ cm}^{-3}$ and $V_{th,i} \approx 100$ km/s; (c) Magnetosphere— $N_{i,m-sph} \approx 2.40 \text{ cm}^{-3}$ and $V_{th,i} \approx 100$ km/s Figure 10 shows 2-D cuts of the density for the cloud, magnetospheric and magnetosheath plasma. The plasma cloud penetrates deeper into the magnetosphere and there is an expansion of the plasma cloud in the Z direction producing a wide depletion of the magnetospheric

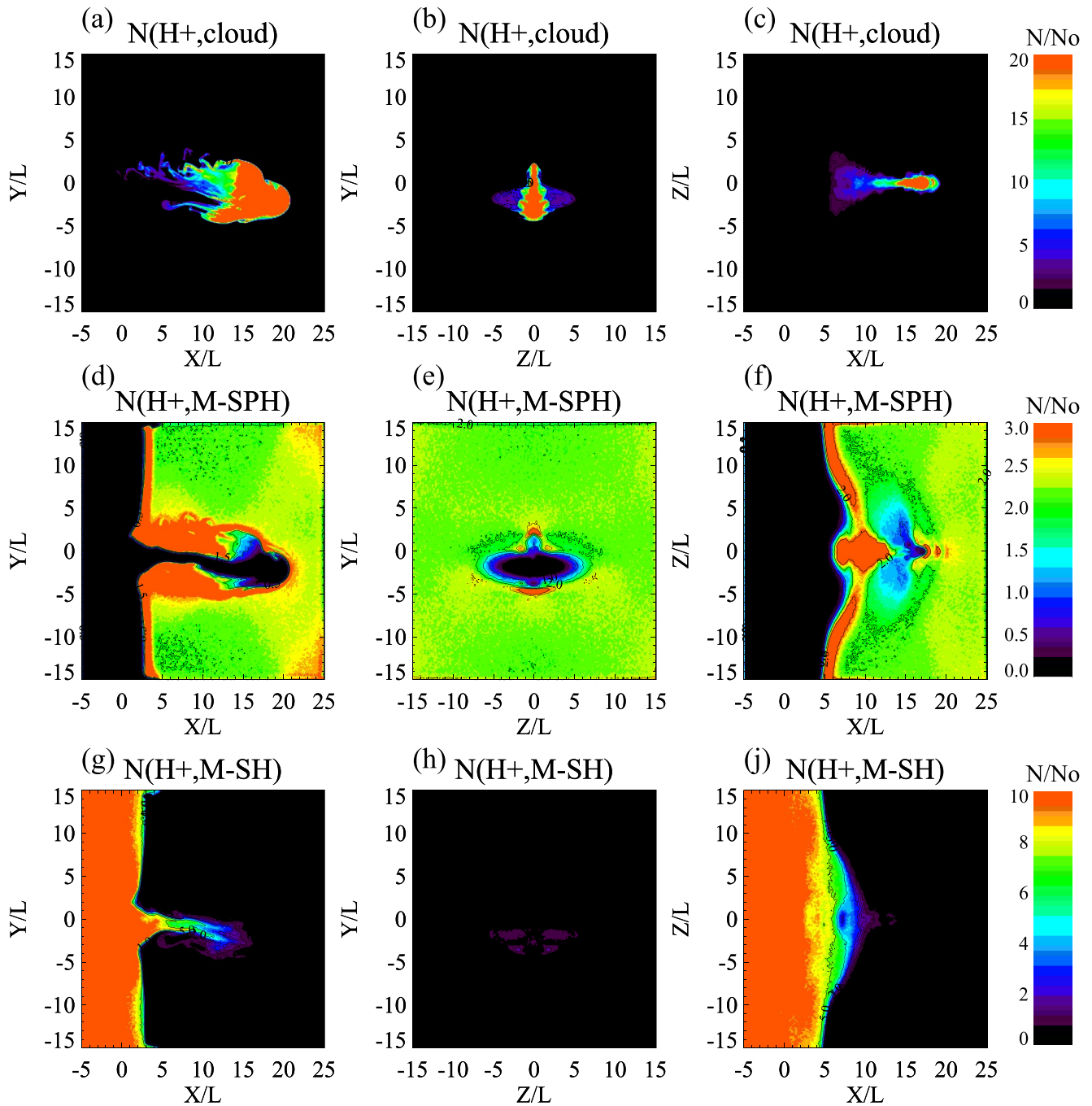


Figure 8. Low density magnetosheath and fast initial P-C speed (Case 2, Run 52ghcc). Top: Cloud density; Middle: Magnetospheric density; Bottom: Magnetosheath density. $L = 400$ km; Cloud speed $U_x = 700$ km/s; initial plasma density and ion thermal velocity: (a) Plasma cloud: $N_{i,cloud} \approx 110 \text{ cm}^{-3}$; $V_{th,i} \approx 10$ km/s; (b) Magnetosheath: $N_{i,m-sh} \approx 10 \text{ cm}^{-3}$; $V_{th,i} \approx 147$ km/s; (c) Magnetosphere: $N_{i,m-sph} \approx 2.4 \text{ cm}^{-3}$; $V_{th,i} \approx 100$ km/s. The middle column is located at $X \approx 16 L$ and $t \approx 16.7$ s.

plasma in that direction. The front of the TD expands in the X direction in the X - Z plane whereas it expands in the opposite direction in the X - Y plane.

3.3. Wave-Particle Interactions Under Plasma Cloud Penetration via TD

This section considers the wave-particle interactions between the plasma cloud and the ambient plasma. Figure 11 presents the evolution of the plasma cloud configuration with time. At the early stage the plasma cloud becomes a

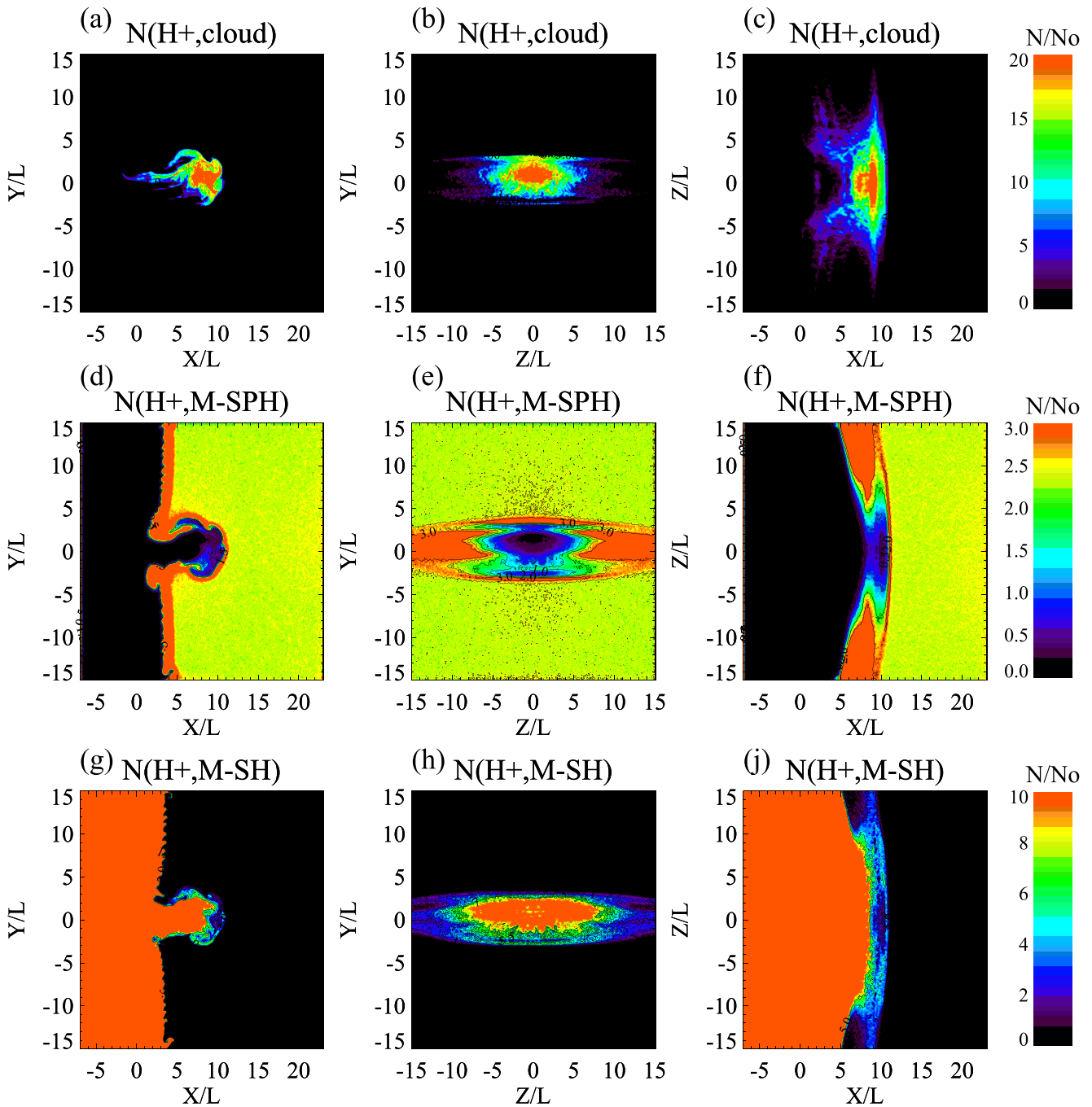


Figure 9. Dense magnetosheath and moderate initial P–C speed but short initial distance to MP (Case 3, Run 120ghkhbb). Top: Cloud density; Middle: Magnetospheric density; Bottom: Magnetosheath density. $L = 200$ km; Cloud speed $U_x = 300$ km/s; initial plasma density and ion thermal velocity: (a) Plasma cloud: $N_{i,cloud} \approx 110 \text{ cm}^{-3}$, $V_{th,i} \approx 10$ km/s; (b) Magnetosphere: $N_{i,m-sh} \approx 60 \text{ cm}^{-3}$, $V_{th,i} \approx 60$ km/s; (c) Magnetosheath: $N_{i,m-sh} \approx 2.4 \text{ cm}^{-3}$, $V_{th,i} \approx 100$ km/s. The middle column is located at $X \approx 9 L$ and $t \approx 19.2$ s.

deformed quasi-sphere while it travels and expands inside the magnetosheath ($t < 2.57$ s). At later time ($t > 7.7$ s) the modeling produces the “mushroom-like” structure strongly extended in the Y direction and compressed in the X direction with a very thin plasma wake.

The plasma cloud configuration at the time $t \approx 18.6$ s is now considered in detail. The modeling produces a hat-like mushroom structure that is unlike the shape across the magnetic field in 2.5-D MHD, Hall-MHD and hybrid modeling with a parallel magnetic external field as in Huba (1996) and Savoini et al. (1994). The push of the

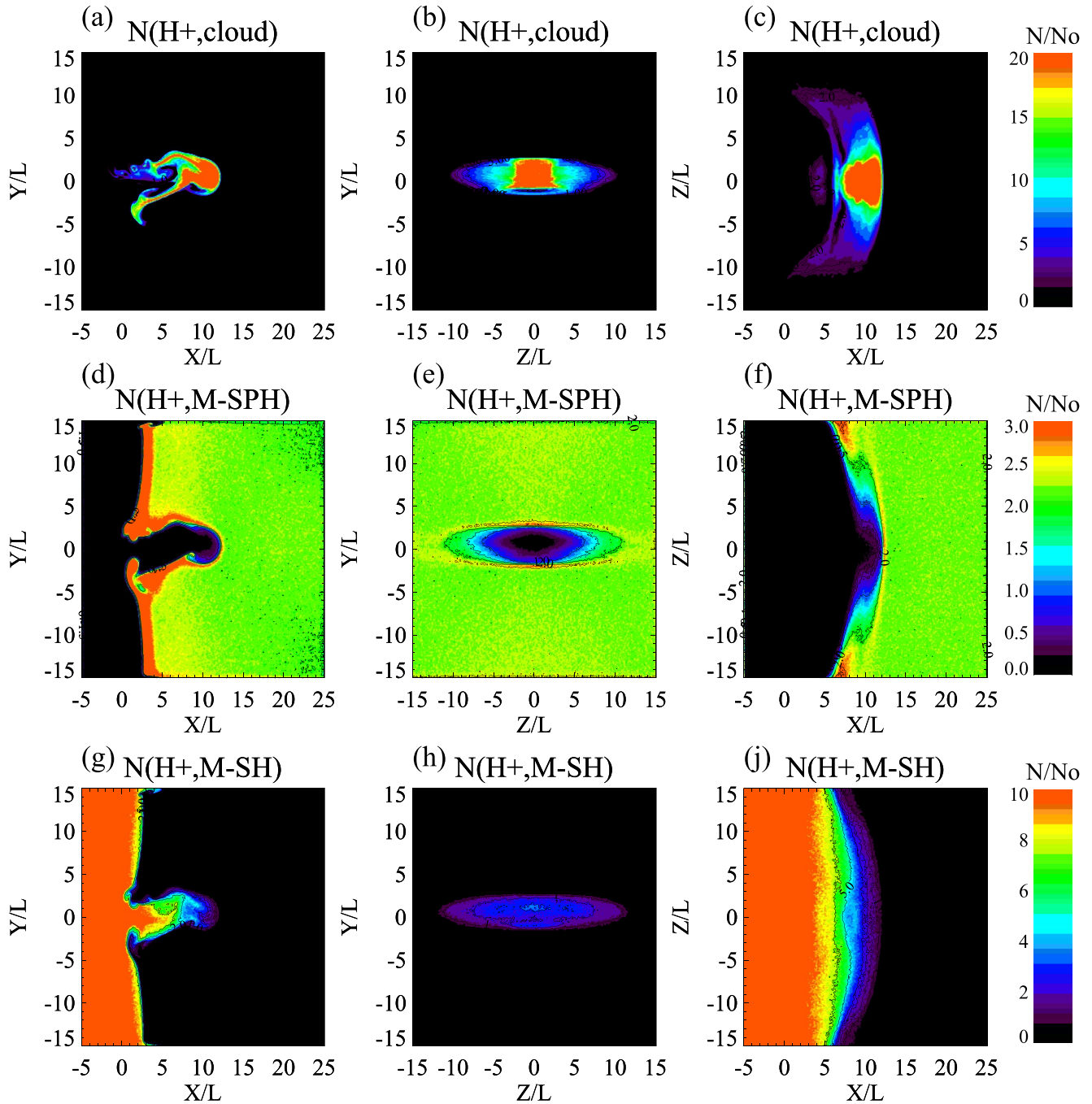


Figure 10. Low magnetosheath density and moderate initial P-C speed (Case 4, Run 80ghjcc). Top: Cloud density; Middle: Magnetospheric density; Bottom: Magnetosheath density. $L = 400$ km; Cloud speed $U_x = 350$ km/s; initial plasma density and ion thermal velocity: (a) Plasma cloud: $N_{i,cloud} \approx 110 \text{ cm}^{-3}$; $V_i \approx 10$ km/s; (b) Magnetosheath: $N_{i,m-sh} \approx 10 \text{ cm}^{-3}$; $V_i \approx 147$ km/s; (c) Magnetosphere: $N_{i,m-sph} \approx 2.4 \text{ cm}^{-3}$; $V_i \approx 100$ km/s. The middle column is located at $X \approx 10 L$ and $t \approx 19.5$ s.

plasma cloud through the ambient magnetosheath and magnetospheric plasma can result in Rayleigh–Taylor (interchange) instabilities at the interface between those plasmas. The modeling shows the formation of a deformed mushroom head-like a curved asymmetrical plate - with a thickness of $1.76 L = 352$ km in the middle part and of $3.5 L = 700$ km in the peripheral regions. Estimates of the density gradient length near the lobe interface between the plasma cloud and magnetospheric plasma, and the ratio between the ion gyroradius and density gradient length yield the following: $L_n = (\partial \ln(n)/\partial x)^{-1} \approx 0.1 L$ and $r_{ci}/L_n > 1.66$ for the ion thermal velocity $V_{i,th} > 100$ km/s. According to Ripin et al. (1993) and Huba et al. (1990) the large Larmor radius (LLR)

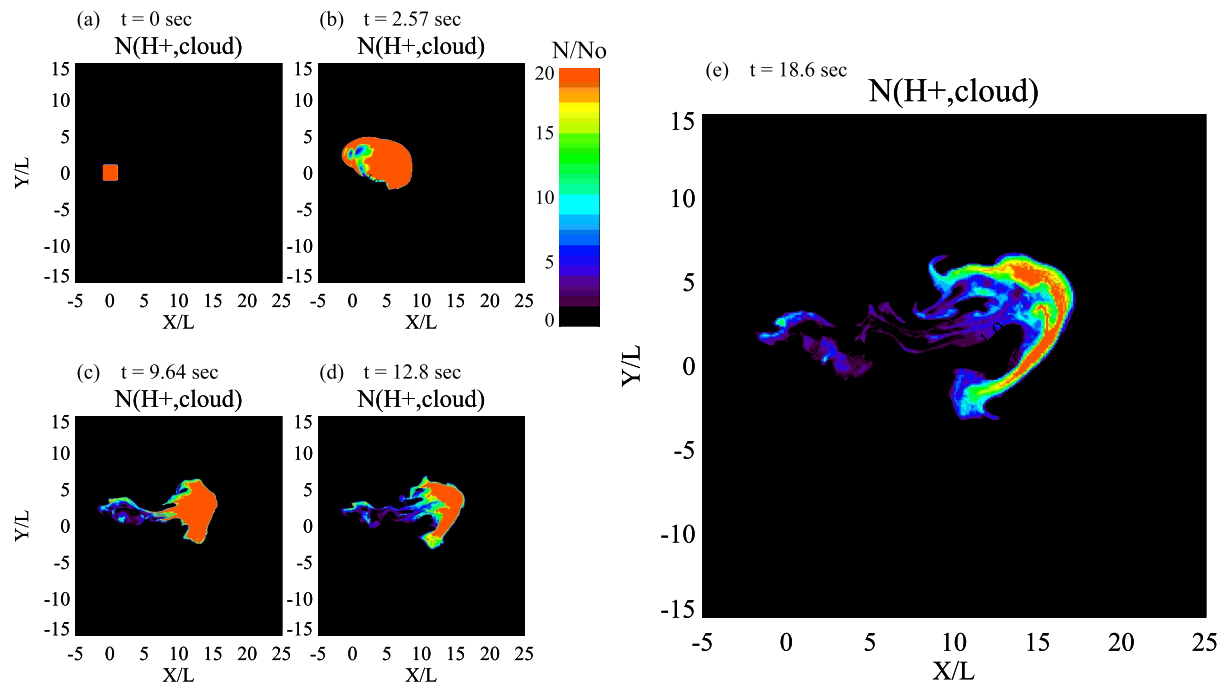


Figure 11. Time evolution of the 2-D cuts of the plasma cloud density configuration in the X - Y plane.

effect will play an important role in the Rayleigh–Taylor instability. Our modeling shows density clumping due to instabilities in the long wavelength ($2\pi L_n/\lambda \ll 1$) in the mushroom-like head.

The modeling also demonstrates oscillations in the wake structure of the plasma cloud with a wavelength of $\lambda \approx (4.2\text{--}4.5) L$ and amplitude of $2.5 L$, where $L = 200$ km. Such waves were not observed in the MHD and Hall-MHD modeling by Huba (1996) in both the parallel and antiparallel magnetic field cases. Weak oscillation in the combined magnetosheath and cloud plasma wake were observed in the 2.5-D hybrid modeling by Savoini et al. (1994) in the antiparallel magnetic field case. The authors suggested that these oscillations may be caused by excitation of the Kelvin-Helmholts instability. Analysis of the modeling results presented in Case 1 (Table 1) shows that each of the 3 plasma species (magnetosheath, plasma cloud and magnetosphere) display a different form of perturbation in the density profiles. Note here that a separate kinetic description is used for each species of ions. These types of perturbations in the plasma cloud wake were also observed in 2.5-D hybrid kinetic modeling of a very weak comet by Lipatov et al. (1997). In the case of an extremely weak gas production rate, the ions move through the wake along the cycloid trajectory because their motion does not disturb the external solar wind flow. The estimation of the plasma cloud ion cycloid motion in the present study yields the following for wavelength and the amplitude of perturbations: $\lambda \approx (3\text{--}7) L$ and the amplitude $2.5 L$ for the external magnetic field 30 nT (magnetosheath) and 60 nT (magnetosphere), and the speed of the plasma cloud of 700 km/s.

The ion velocity distribution of the plasma cloud becomes anisotropic with $T_{i,\perp}/T_{i,\parallel} \geq 9$ due to pickup processes in the plasma system –plasma cloud-magnetosheath and plasma cloud-magnetosphere. Such effect were also observed in solar wind mass loading by the cometary plasma, plasma cloud release in the active experiments in space (Galeev & Lipatov, 1984; Galeev et al., 1985; Winske et al., 1985 and references therein).

The stability of liquid clouds (droplets) in the gas/low density fluid flow limit is a general problem of two-phase flow with many applications in space/meteorology and climate physics, and gas-dynamics systems. The rate of disintegration of the cloud is the key factor in the phase mixing processes between clusters of liquid clouds (droplets) and external/internal flow. One of the main similarities is that the liquid clouds (droplets) strongly deform across the direction of the bulk velocity of the external flow. Such configurations already become unstable and the liquid clouds (droplets) break-up (see e.g. Isshiki, 1959; Volynskii & Lipatov, 1970 and references therein).

3.4. Comparison Between Simulated and Observed Transmitted Plasma Clouds

Our 3-D hybrid modeling reveals essential conditions for plasma cloud penetration across the tangential discontinuity (TD), namely, initial position of the plasma clouds relatively the TD; initial speed of the plasma clouds; the size and configuration of the plasma clouds; the density of the magnetosheath plasma; the density and magnetic field in the magnetospheric plasma near TD; and the local speed of the TD. It is difficult to predict the potential of plasma cloud penetration through the TD on the basis of spacecraft observations because the plasma system under investigation is controlled by multiple key parameters (see Table 1).

Our simulations give an ion flux of $\approx 4 \times 10^8 \text{ (cm}^2 \text{ s)}^{-1}$ inside the leading end of the plasma cloud (Case 1, Run—ghkhha, Table 1) and $\approx 16 \times 10^8 \text{ (cm}^2 \text{ s)}^{-1}$ (Case 2, Run—ghcc, Table 1) for the initial plasma cloud speed of 700 km/s. The simulations with smaller initial plasma cloud speeds 300 km/s and 350 km/s give ion fluxes of $\approx 4 \times 10^8 \text{ (cm}^2 \text{ s)}^{-1}$ (Case 3, Run—ghkhbb, Table 1) and $\approx 3 \times 10^8 \text{ (cm}^2 \text{ s)}^{-1}$ (Case 4, Run—ghjcc, Table 1).

Dmitriev and Suvorova (2015) estimated an ion flux of $3 \times 10^8 \text{ (cm}^2 \text{ s)}^{-1}$ in the penetrating plasma clouds (plasmoids) with a speed of $\approx 220 \text{ km/s}$ which is based on the THEMIS observations. They concluded that plasma cloud (plasmoid) penetrations across the magnetopause were observed in cases with $\beta_k > 1$ and $U > 220 \text{ km/s}$. Here, the kinetic plasma beta is $\beta_k = \frac{1}{2} M_i U^2 / (B^2 / 8\pi)$. There were no observations of plasma cloud penetrations via the magnetopause in cases with $\beta_k > 1$ and $U > 250 \text{ km/s}$. Lyatsky et al. (2016) used Cluster observations and found separated filaments inside the magnetosphere with parameters that are close to the magnetosheath plasma with speed of $U_x \approx 100\text{--}200 \text{ km/s}$. In some cases near the subsolar region they also found filaments with $U_x \approx 300\text{--}400 \text{ km/s}$. The density inside the filament was 10 cm^{-3} and its value is about the same as the density inside the magnetosheath. They also showed that the velocity and density inside the filaments is inhomogeneous. Those results are in agreement with the hybrid modeling presented here.

Analysis of the MMS observations show the existence of moving plasma clouds behind the magnetopause. In Lipatov et al. (2022) it was assumed that these clouds are created by FTEs inside the magnetopause due to magnetic reconnection (Akhavan et al., 2018). However, the clouds created by FTEs may also be pushed into the magnetosheath where they will then be transferred to the magnetosphere across the magnetopause. MMS spacecraft data analysis gives the following parameters for observed clouds: speed is of (250–500) km/s; density is of (20–60) cm^{-3} ; and the ion temperature is of (500–1,800) eV. Note that these values are close to the parameters of the plasma clouds observed in hybrid kinetic simulation. The strong deformation of the plasma cloud due to the Rayleigh-Taylor instability presented in this paper have not yet been observed in the observations.

4. Conclusions

The data analysis from the MMS spacecraft with time-resolution 150 ms for ions and 30 ms for electrons along with 3-D hybrid kinetic simulation are used to provide, for the first time, insights into the wave-particle interactions triggered by penetrations of plasma clouds into the magnetosphere via the magnetopause considered as a tangential discontinuity. The main results are:

- Plasma cloud dynamics are controlled mainly by the initial speed of the plasma clouds, the ratio of the plasma cloud/magnetosheath plasma density, and the ratio of the magnetospheric and magnetosheath magnetic field. For typical plasma parameters of the magnetosheath and magnetosphere the plasma cloud with initial speed 700 km/s freely penetrates the magnetopause (see Table 1). Plasma clouds with initial speed of 300–350 km/s can penetrate the magnetopause only in cases with sufficiently low magnetosheath density or in cases when the initial position of the plasma clouds is close enough to the magnetopause (see Table 1);
- The initial distance between the plasma cloud and magnetopause is also a critical parameter and determines the amount of magnetosheath plasma will be transferred into the magnetosphere (see Table 1);
- The performed modeling provides further understandings of the physics of penetration of the solar wind filamentary plasma elements, moons, and comets (see e.g. Shoemaker-Levy 9 comet interaction with Jupiter modeling by Lipatov & Sharma, 1994) through the planetary bow shock and magnetopause.
- The modeling may be important for understanding the penetration of plasma clouds via the heliopause.

Followup work will investigate: Plasma cloud penetration through the TD with antiparallel magnetic fields; effects of magnetic reconnection on plasma cloud dynamics; and plasma cloud penetration through rotational discontinuities (RD); and effects of plasma cloud penetration on global plasma and magnetic field perturbations

inside the magnetopause. Future modeling will be performed for various initial thicknesses of the magnetopause (TD and RD) and various values of anomalous resistivity inside the magnetopause. The investigations will also be performed for ellipsoid-like plasma clouds and non-zero initial bulk velocities of the magnetosheath and magnetospheric plasmas.

Data Availability Statement

This research was supported by the National Aeronautics and Space Administration (NASA) Magnetospheric Multiscale Mission. Computational resources were provided by NASA Advances Supercomputing Division (Ames Research Center - Aitken supercomputer) via SMD-20-87113888 Project. MMS data is publicly available at the Science Data Center (<https://lasp.colorado.edu/mms/sdc/public/>). Observation data from the WIND spacecraft were downloaded from CDAWeb (https://cdaweb.gsfc.nasa.gov/cdaweb/istp_public/) and provided by A. Szabo, R. Lin, S. Bale, and K. Ogilvie. A.S.L. was also supported in part by NASA Award 80NSSC20K0146 to UMBC from the NASA Solar System Workings Research Program (SSW-2018) and JCET UMBC Project CV388766.

Acknowledgments

This research was supported by the National Aeronautics and Space Administration (NASA) Magnetospheric Multiscale Mission. Computational resources were provided by the NASA Advanced Supercomputing Division in Ames Research Center (Aitken-Rome supercomputer) via SMD-20-87113888 Project. A.S.L. was also supported in part by Award 80NSSC20K0146 to UMBC from NASA Solar System Workings Research Program (SSW2018) and JCET UMBC Project CV388766. The MMS L2 data used in this paper, can be accessed from MMS Science Data - Center (<https://lasp.colorado.edu/mms/sdc/public/>).

References

- Akhavan-Tafti, M., Slavin, J. A., Le, G., Eastwood, J. P., Strangeway, R. J., Russell, C. T., et al. (2018). MMS examination of FTEs at the Earth's subsolar magnetopause. *Journal of Geophysical Research: Space Physics*, 123(2), 1224–1241. <https://doi.org/10.1002/2017ja024681>
- Amata, E., Savin, S. P., Ambrosino, D., Bogdanova, Y. V., Marcucci, M. F., Romanov, S., & Skalsky, A. (2011). High kinetic energy density jets in the Earth's magnetosheath: A case study. *Planetary and Space Science*, 59(7), 482–494. <https://doi.org/10.1016/j.pss.2010.07.021>
- Archer, M. O., Hurbury, T. S., & Eastwood, J. P. (2012). Magnetosheath pressure pulses: Generation downstream of the bow shock from solar wind discontinuities. *Journal of Geophysical Research*, 117(A5), A05228. <https://doi.org/10.1029/2011JA017468>
- Bashurin, V. P., Golubev, A. I., & Terekhin, V. A. (1983). The collisionless deceleration of an ionized cloud dispersing in a uniform plasma in a magnetic field. *Journal of Applied Mechanics and Technical Physics*, 24(5), 614–620. <https://doi.org/10.1007/bf00905870>
- Berezin, Y. A., Vshivkov, V. A., Dudnikova, G. I., & Fedoruk, M. P. (1992). Collisionless slowing down of a plasma cloud in a nonuniform magnetized background. *Soviet Journal of Plasma Physics*, 18(12), 1567.
- Braginskii, S. L. (1965). Transport processes in a plasma. In M. A. Leontovich (Ed.), *Reviews of plasma physics* (pp. 205–240). Consultants Bureau.
- Burch, J. L., Moore, T. E., Torbert, R. B., & Giles, B. L. (2016). Magnetospheric multiscale overview and science objectives. *Space Science Reviews*, 199(1–4), 5–21. <https://doi.org/10.1007/s11214-015-0164-9>
- Cowley, S. W. H. (1986). The impact of recent observations on theoretical understanding of solar wind-magnetosphere interactions. *Journal of Geomagnetism and Geoelectricity*, 38(11), 1223–1256. <https://doi.org/10.5636/jgg.38.1223>
- Dai, W., & Woodward, P. R. (1994). Two-dimensional simulations for the impulsive penetration of a solar wind filament into the magnetosphere. *Journal of Geophysical Research*, 99(A5), 8577–8584. <https://doi.org/10.1029/93ja03026>
- Dai, W., & Woodward, P. R. (1995). Interactions between a solar wind filament and an open magnetosphere. *Journal of Geophysical Research*, 100(A8), 14843–14852. <https://doi.org/10.1029/94ja02630>
- Dmitriev, A. V., & Suvorova, A. V. (2015). Large-scale jets in the magnetosheath and plasma penetration across the magnetopause: THEMIS observations. *Journal of Geophysical Research: Space Physics*, 120(6), 4423–4437. <https://doi.org/10.1002/2014JA020953>
- Escoubet, C. P. H., Hwang, K.-J., Toledo-Redondo, S., Turc, L., Haaland, S. E., Aunai, N., et al. (2020). Cluster and MMS simultaneous observations of magnetosheath high speed jets and their impact on the magnetopause. *Frontiers in Astronomy and Space Science*, 6(78). <https://doi.org/10.3389/fspas.2019.00078>
- Galeev, A. A., & Lipatov, A. S. (1984). Plasma processes in cometary atmospheres. *Advances in Space Research*, 4(9), 229–237. [https://doi.org/10.1016/0273-1177\(84\)90034-6](https://doi.org/10.1016/0273-1177(84)90034-6)
- Galeev, A. A., Lipatov, A. S., & Sagdeev, R. Z. (1985). Numerical simulation of shock waves near comets: Structural features and energy dissipation mechanisms. *Soviet Physics Journal of Experimental and Theoretical Physics*, 62(5), 866.
- Gunell, H., Hurtig, T., Nilsson, H., Koepke, M., & Brenning, N. (2008). Simulations of a plasmoid penetrating a magnetic barrier. *Plasma Physics and Controlled Fusion*, 50(7), 074013. <https://doi.org/10.1088/0741-3335/50/7/074013>
- Gunell, H., Walker, J. J., Koepke, M. E., Hurtig, T., Brenning, N., & Nilsson, H. (2009). Numerical experiments on plasmoids entering a transverse magnetic field. *Physics of Plasmas*, 16(11), 112901. <https://doi.org/10.1063/1.3267860>
- Heikkilä, W. J. (1982). Impulsive plasma transport through the magnetopause. *Geophysical Research Letters*, 9(2), 159–162. <https://doi.org/10.1029/GL009i002p00159>
- Hietala, H., Laitinen, T. V., Andreeva, K., Vainio, R., Vaivads, A., Palmroth, M., et al. (2009). Supermagnetosonic jets behind a collisionless quasiparallel shock. *Physical Review Letters*, 103(24), 245001. <https://doi.org/10.1103/PhysRevLett.103.245001>
- Hietala, H., & Plaschke, F. (2013). On the generation of magnetosheath high-speed jets by bow shock ripples. *Journal of Geophysical Research: Space Physics*, 118(11), 7237–7245. <https://doi.org/10.1002/2013JA019172>
- Huba, J. D. (1996). Impulsive plasmoid penetration of a tangential discontinuity: Two-dimensional ideal and Hall magnetohydrodynamics. *Journal of Geophysical Research*, 101(A11), 24855–24868. Paper number 96JA02563. <https://doi.org/10.1029/96ja02563>
- Huba, J. D., Hassam, A. B., & Winske, D. (1990). Stability of sub-Alfvénic plasma expansions. *Physics of Fluids B*, 2(7), 1676–1697. <https://doi.org/10.1063/1.859441>
- Isshiki, N. (1959). Theoretical and experimental study of atomization of liquid drop in high-speed gas stream. *Rep. Transp. Techn. Research Inst.*, 35.
- Jarvinen, R., Vainio, R., Palmroth, M., Juusola, L., Hoilijoki, S., Pfau-Kempf, Y., et al. (2018). Ion acceleration by flux transfer events in the terrestrial magnetosheath. *Geophysical Research Letters*, 45(4), 1723–1731. <https://doi.org/10.1002/2017GL076192>
- Lemaire, J. (1977). Impulsive penetration of filamentary plasma the magnetospheres of the Earth and Jupiter. Research Note. *Planetary and Space Science*, 25(9), 887–890. [https://doi.org/10.1016/0032-0633\(77\)90042-3](https://doi.org/10.1016/0032-0633(77)90042-3)

- Lemaire, J. (1985). Plasmoid motion across a tangential discontinuity (with application to the magnetopause). *Journal of Plasma Physics*, 33(3), 425–436. <https://doi.org/10.1017/s0022377800002592>
- Lemaire, J., & Roth, M. (1978). Penetration of solar wind plasma elements into the magnetosphere. *Journal of Atmospheric and Terrestrial Physics*, 40(3), 331–335. [https://doi.org/10.1016/0021-9169\(78\)90049-1](https://doi.org/10.1016/0021-9169(78)90049-1)
- Lipatov, A. S. (1996). 3-D and 2.5-D hybrid multiscale simulation technology: Application to study of forced nonstationary processes at tangential discontinuities. *STEP SIMPO Newsletter*, 5(16), 11–15.
- Lipatov, A. S. (2002). *The hybrid multiscale simulation technology. An introduction with application to astrophysical and laboratory plasmas, scientific computation*. (pp. 1–403). Springer-Verlag. Retrieved from www.Springer.com
- Lipatov, A. S. (2012). Merging for particle-mesh complex particle kinetic modeling of the multiple plasma beams. *Journal of Computational Physics*, 231(8), 3101–3118. <https://doi.org/10.1016/j.jcp.2011.12.020>
- Lipatov, A. S., Avakov, L. A., & Giles, B. L. (2022). Hybrid kinetic model of the interaction between the dense plasma clouds and magnetospheric plasma on large time and spatial scales, and comparison with MMS observations. *Journal of Geophysical Research - Space Physics*, 127(7), e2022JA030493. <https://doi.org/10.1029/2022JA030493>
- Lipatov, A. S., Avakov, L. A., Giles, B. L., & Gershman, D. J. (2024). Hybrid Kinetic Model of the magnetosheath plasma cloud penetration through the magnetopause and comparison with MMS observations. Preliminary results. *ESS Open Archive*. <https://doi.org/10.1029/2024JA032909>
- Lipatov, A. S., Martinez, C., Motschmann, U., Glaumeier, K.-H., & Fränz, M. (2006). The study of the interaction of the solar wind with Venus: 3D hybrid model. Progress Report for the DFG Grant 436 RUS 17/81/06 from the Deutsche Forschungsgemeinschaft.
- Lipatov, A. S., Motschmann, U., Bagdonat, T., & Griaumeier, J.-M. (2005). The interaction of the stellar wind with an extrasolar planet—3D hybrid and drift-kinetic simulations. *Planetary and Space Science*, 53(4), 423–432. <https://doi.org/10.1016/j.pss.2004.11.001>
- Lipatov, A. S., Sauer, K., & Baumgärtel, K. (1997). 2.5-D hybrid code simulation of the solar wind interaction with weak comets and related objects. *Advances in Space Research*, 20(2), 219–282. [https://doi.org/10.1016/s0273-1177\(97\)00547-4](https://doi.org/10.1016/s0273-1177(97)00547-4)
- Lipatov, A. S., & Sharma, A. S. (1994). Hybrid simulation of comet Shoemaker-Levy 9 interaction with Jovian bow shock. *Geophysical Research Letters*, 21(11), 1059–1062. <https://doi.org/10.1029/94gl01295>
- Lipatov, A. S., Sharma, A. S., & Papadopoulos, K. (1994). *Two-dimensional hybrid simulation of whistler and Alfvén wave generated by plasma beams in tangential discontinuities*. University of Maryland Department of Astronomy Report.
- Lipatov, A. S., & Sibeck, D. G. (2020). Concerning the interaction of a transmitted interplanetary impulse with a plasmaspheric drainage plume: First results from 3-D hybrid kinetic modeling. *Planetary and Space Science*, 194, 105104. <https://doi.org/10.1016/j.pss.2020.105104>
- Lundin, R., & Dubinin, E. (1984). Solar wind energy transfer regions inside the dayside magnetopause—I. Evidence for magnetosheath plasma penetration. *Planetary and Space Science*, 32(6), 745–755. [https://doi.org/10.1016/0032-0633\(84\)90098-9](https://doi.org/10.1016/0032-0633(84)90098-9)
- Lyatsky, W., Pollock, C., Goldstein, M. L., Lyatskaya, S., & Avakov, L. (2016). Penetration of the magnetosheath plasma into dayside magnetosphere: I. Density, Velocity, and rotation. *J. Geophys. Res.*, 121(8), 7699–7712. <https://doi.org/10.1002/2015JA022119>
- Ma, Z. W., Hawkins, J. G., & Lee, L. C. (1991). A simulation study of impulsive penetration of solar wind irregularities into the magnetosphere at the dayside magnetopause. *J. Geophys. Res.*, 96(A9), 15751–15765. <https://doi.org/10.1029/91ja01322>
- Nemecék, Z., Safrankova, J. M., Prech, L., Sibeck, D. G., Kokubun, S., Mukai, T., et al. (1998). Transient flux enhancements in the magnetosheath. *Geophysical Research Letters*, 25(8), 1273–1276. <https://doi.org/10.1029/98GL50873>
- Omidi, N., Berchem, J., Sibeck, D., & Zhang, H. (2016). Impacts of spontaneous hot flow anomalies on the magnetosheath and magnetopause. *Journal of Geophysical Research: Space Physics*, 121(4), 3155–3169. <https://doi.org/10.1002/2015JA022170>
- Owen, C. J., & Cowley, S. W. H. (1991). Heikkilä's mechanism for impulsive plasma transport through the magnetopause: Reexamination. *Journal of Geophysical Research*, 96, 5565.
- Palmroth, M., Raptis, S., Suni, J., Karlsson, T., Turc, L., Johlander, A., et al. (2021). Magnetosheath jet evolution as a function of lifetime: Global hybrid-Vlasov simulations compared to MMS observations. *Annals of Geophysics*, 39(2), 289–308. <https://doi.org/10.5194/angeo-39-289-2021>
- Plaschke, F., Hietala, H., Angelopoulos, V., & Nakamura, R. (2016). Geoeffective jets impacting the magnetopause are very common. *Journal of Geophysical Research: Space Physics*, 121(4), 3240–3253. <https://doi.org/10.1002/2016JA022534>
- Pollock, C., Moore, T., Jacques, A., Burch, J., Gliese, U., Saito, Y., et al. (2016). Fast plasma investigation for magnetospheric multiscale. *Space Science Reviews*, 199(1), 331–406. <https://doi.org/10.1007/s11214-016-0245-4>
- Prokopov, P. A., Zakharov, Y. P., Tishchenko, V. N., Shaikhislamov, I. F., Boyarintsev, E. L., Melekhov, A. V., et al. (2016). Laser plasma simulations of the generation processes of Alfvén and collisionless shock waves in space plasma. *Journal of Physics: Conference Series*, 769, 012086. <https://doi.org/10.1088/1742-6596/769/1/012086>
- Ripin, B. H., Huba, J. D., McLean, E. A., Manka, C. K., Peyser, T., Burris, H. R., & Grun, J. (1993). SubAlfvénic plasma expansion. *Physics of Fluids B: Plasma Physics*, 5(10), 3491–3506. <https://doi.org/10.1063/1.860825>
- Russell, C. T., Anderson, B. J., Baumjohann, W., Bromund, K., Dearborn, D., Fischer, D., et al. (2016). The magnetospheric multiscale magnetometers. *Space Science Reviews*, 199(1), 189–256. <https://doi.org/10.1007/s11214-014-0057-3>
- Savin, S., Amata, E., Zelenyi, L., Budaev, V., Consolini, G., Treumann, R., et al. (2008). High kinetic energy jets in the earth's magnetosheath: Implications for plasma dynamics and anomalous transport. *JETP Letters (Translation of Pis'ma v Zhurnal Eksperimental'noi i Teoreticheskoi Fiziki)*, 87(11), 593–599. <https://doi.org/10.1134/S0021364008110015>
- Savoini, P., Scholer, M., & Fujimoto, M. (1994). Two-dimensional hybrid simulations of impulsive plasma penetration through a tangential discontinuity. *Journal of Geophysical Research*, 99(A10), 19377–19391. <https://doi.org/10.1029/94ja01512>
- Schindler, K. (1979). On the role of irregularities in plasma entry into the magnetosphere. *Journal of Geophysical Research*, 84(A12), 7257–7266. <https://doi.org/10.1029/JA084iA12p07257>
- Schot, S. H. (1992). Eighty years of Sommerfeld's radiation condition. *Historia Mathematica*, 19(4), 385–401. [https://doi.org/10.1016/0315-0860\(92\)90004-u](https://doi.org/10.1016/0315-0860(92)90004-u)
- Shue, J.-H., Chao, J.-K., Song, P., McFadden, J. P., Suvorova, A., Angelopoulos, V., et al. (2009). Anomalous magnetosheath flows and distorted subsolar magnetopause for radial interplanetary magnetic fields. *Geophysical Research Letters*, 36(18), L18112. <https://doi.org/10.1029/2009GL039842>
- Suzuki, Y., Watanabe, T.-H., Kageyama, A., Sato, T., & Hayashi, T. (1998). Three-dimensional simulation study of plasmoid injection into magnetized plasma. In K. Koyama, S. Kitamoto, M. Itoh, & Symposium - International Astronomical Union. (Eds.), *The hot Universe. International Astronomical union/unión Astronomique Internationale*, (Vol. 188, pp. 209–210). Springer. <https://doi.org/10.1007/978-94-011-4970-9/49>

- Voitcu, G., & Echim, M. (2016). Transport and entry of plasma clouds/jets across transverse magnetic discontinuities: Three-dimensional electromagnetic particle-in-cell simulations. *Journal of Geophysical Research: Space Physics*, 121(5), 4343–4361. <https://doi.org/10.1002/2015JA021973>
- Volynskii, M. S., & Lipatov, A. S. (1970). Deformation and disintegration of liquid droplets in a gas flow. *Journal of Engineering Physics and Thermophysics*, 18(5), 579–583. <https://doi.org/10.1007/BF00829386>
- Winske, D., Wu, C. S., Li, Y. Y., Mou, Z. Z., & Guo, S. Y. (1985). Coupling of newborn ions to the solar wind by electromagnetic instabilities and their interaction with the bow shock. *Journal of Geophysical Research*, 90(A3), 2713–2726. <https://doi.org/10.1029/ja090ia03p02713>